**OPTICAL FLOW BASED SUPER-RESOLUTION RESTORATION OF LRO NAC REPEAT-PASS IMAGERY OF THE CHANG'E-3 LANDING SITE.** W. L. Chen[1, 2], J. J. Liu[1, 2], H. B. Zhang[1, 2], D. W. Liu[1, 2], X. X. Zhang[1, 2], X. Y. Gao[1, 2], C. L. Li[1, 2], [1]National Astronomical Observatories, Chinese Academy of Sciences, Beijing, China (chenwl@nao.cas.cn), [2]Key Laboratory of Lunar and Deep Space Exploration, Chinese Academy of Sciences, Beijing, China.

**Introduction:** High spatial resolution imaging data is always desired for lunar and planetary science, especially in the research branch of planetary topography and morphology. Image resolution describes the details in an image, the higher the resolution is, the more image details can be used to improve understanding of the planetary surface formation processes.

As a stage of the Chinese Lunar Exploration Program (CLEP), the Chang'E-3 probe, which included a lander and a rover, landed successfully at $44.12^{o}$ N, $19.51^{o}$ W on Mare Imbrium of the moon on December 14, 2013. So it is necessary and intriguing to know more about this area for us. LRO passed over the Chang'E-3 landing site repeatedly, and the narrow angle camera (NAC) acquired images of this region with a resolution of 1.5m/pixel, which is the highest-resolution data so far. With these repeat-pass images, we can further enhance the image resolution using the computational imaging technology called super-resolution (SR) restoration. SR takes advantage of the non-redundant sub-pixel information contained in multiple low resolution (LR) images to restore a high resolution (HR) image.

**Method:** SR restoration is the inverse process of observation model of a real imaging system. In general, let $X$ denote the HR image desired, and $y_k$ be the k$^{th}$ LR observation, then image observation model can be expressed by

$$y_k = D_k H_k F_k X + N_k, k = 1, 2, ..., K \qquad (1)$$

where $F_k$ encodes the motion field for the k$^{th}$ frame, $H_k$ models the blurring effects, $D_k$ is the down-sampling operator, and $N_k$ is the noise term. For simplicity, it is usually assumed that $D_k = D$, $H_k = H$, and $N_k = N$. In this research we use the SR model proposed in [1].

In SR model, the motion field means registration from HR image to LR images, which is used to align the non-redundant sub-pixel information in LR images. In some researches, it is assumed that the motion field is known as a priori. If not, this motion information can be estimated easily by employing parametric motion estimation techniques if the scene is rigid and planar. However, planet's surface is heavily cratered, and the motion fields of repeat-pass images are definitely related to imaging perspective and fluctuation of the surface. It means that parametric motion model can not achieve a registration of NAC repeat-pass images with subpixel accuracy. One solution for solving the registration of non-planar images is to allow the registration to be an arbitrary flow field. Although the idea of treating registration in SR to be an arbitrary motion field is not novel[2][3], there are few studies using this method for SR of remote sensing images which are highly non-planar.

The flow chart of our method is shown in Fig 1. The fist step of pre-processing consists of two components:

- enlargement of original LR images to the desired size using simple interpolation techniques, such as bicubic,
- correction of gray difference among repeat-pass remote sensing images which is caused by different imaging time and different view angle.

The Brox's method proposed in [4] is employed for optical flow estimation. It is widely used in the field of computer vision attributing to high accuracy and robustness. More important, a gradient constancy assumption which allows small variations in gray value of multi-frame images is introduced in Brox's method. This makes the method robust to the gray difference among repeat-pass images, although it has been relieved to some extent by gray value correction. In this step, one of the input images is chosen as reference, and optical flow fields from the reference to other images are estimated. As soon as the flow fileds are obtained, all the non-reference images can be warped to the reference one. Then all these aligned images are merged by median filter, and used as the initial value of HR image. The unknow point spread function (PSF) is assumed to be a Gaussian kernel which is usually used to model the comprehensive effect of multiple factoros leading to blur of remote sensing images. And the parameters of Gaussian kernel are selected by experience. Along with the renewal of HR image, flow fields are also updated taking the latest estimated HR image as reference, until the fixed threshold is reached.

**Experiments:** The experimental area is shown in Fig 2. Eight repeat-pass NAC images covering this area after January 21 2014 are used in our experiments. These images with a resolution of 1.5m are processed to solve a 0.8m resolution of the area. Fig 3 shows partial region of the experimental area. Fig 3 (a) is the LRO NAC image which is resized by bicubic interpolation with a scale of 2, and (b) is the SR image with the same scale. The result shows that the quality of NAC image is greatly enhanced and more details are presented in the restored image. Same small craters which are obscure or invisible in (a) are clear and identifiable in (b). Besides, some undesirable textures are also found in Fig 3 (b), we think this is attributed to quantization levels of gray values. And we will try to suppress undesirable textures like these in our future work.

Metric Q[5] and LPC[6] are employed to evaluate the results quantitatively (Tab 1). Metric Q and LPC are both no-reference image sharpness metrics, their values drops when the test image becomes blurred. From Tab 1, it is concluded that the SR restored image is better than bicubic interpolated image both with Metric Q value and LPC value. Particularly, the Metric Q value of SR restored result is 1.6 times as much as that of bicubic interpolated result.

In order to confirm that the enhanced details are actually real information, but not artificial textures. The SR restored image is compared with the image of the same area acquired by the descent camera carried on Chang'E-3 (Fig 4). Fig 4(c) is the 2300$^{th}$ image taken by Chang'E-3 descent camera. This image is taken at a altitude of approximately 1,000m and resulting in a spatial resolution of 0.85m. it is found that the enhanced craters in SR image are actually identified in descent camera image. In other words, the restored SR image is comparable with the descent camera image with a resolution of 0.85m.

**References:** [1] Farsiu S. et al. (2004) *IEEE Transactions on Image Processing, 13(10),* 1327–1344. [2] Baker S. and Kanade T. (1999) *Tech. Rep,* CMU-RI-TR-99-36. [3] Elad M. and Feuer A. (1999) *IEEE Transactions on Image Processing, 8(3),* 387–395. [4] Brox T. et al. (2004) *ECCV, 4,* 25-36. [5] Zhu Xiang and Milanfar P. (2009) *IWQME,*64-69. [6] Hania H. et al. (2010) *ICASSP*.

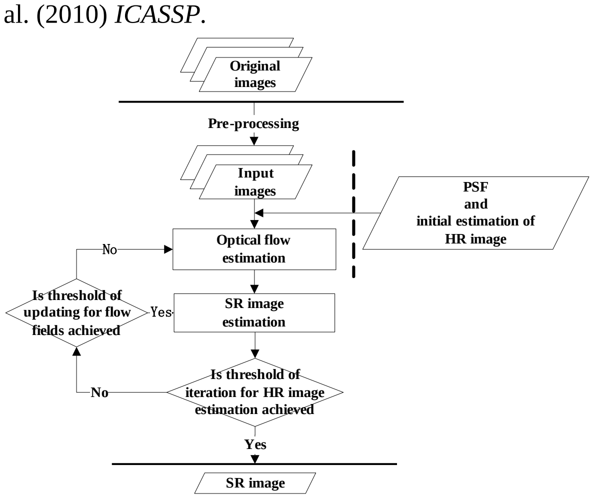


**Figure 1**: Flow chart of the proposed optical flow based super-resolution restoration processing chain.

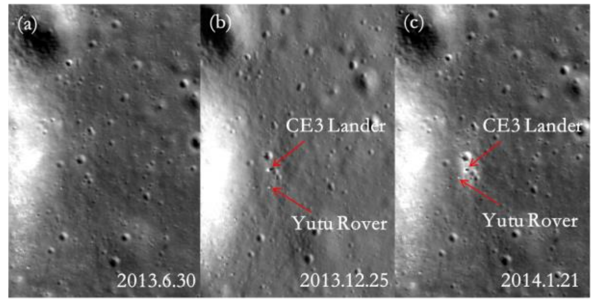


**Figure 2**: (a) LRO NAC image acquired before the landing of Chang'E-3. (b) and (c) LRO NAC images acquired after the landing of Chang'E-3. The arrows point to the location of Chang'E-3 lander and Yutu rover. It is obvious that the location of Yutu rover has changed from December 25 2013 to January 21 2014.

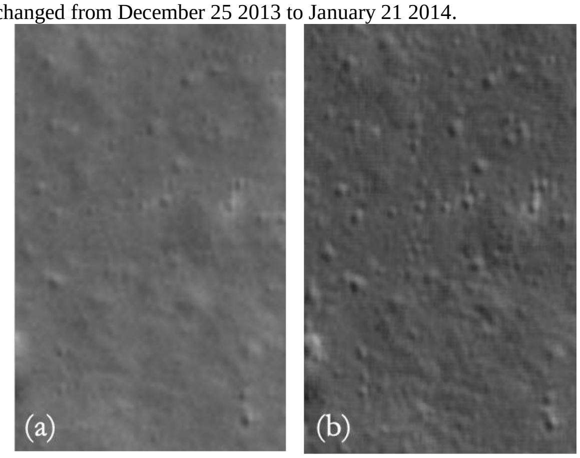


**Figure 3**: (a) LRO NAC image which is resized by bicubic interpolation with a scale of 2. (b) SR image with the same scale.

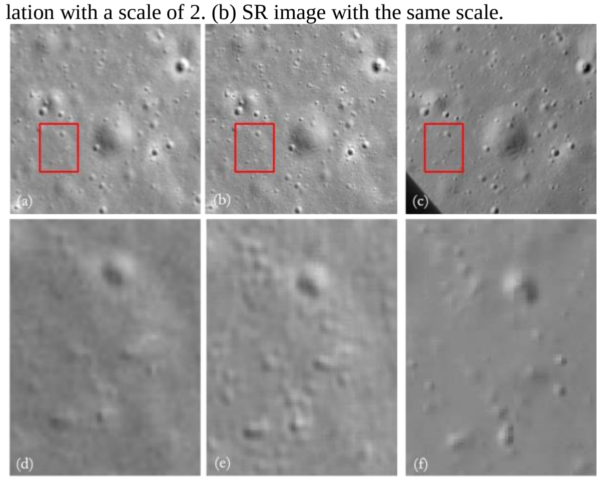


**Figure 4**: (a) LRO NAC image which is resized by bicubic interpolation with a scale of 2. (b) SR image with the same scale. (c) The 2300$^{th}$ image taken by Chang'E-3 descent camera. (d) (e) (f) Details of the area marked by rectangles in (a) (b) and (c) respectively.

**Table 1**: Quantitative comparison of bicubic interpolation and SR restoration results

| | Bicubic interpolation | SR restoration |
|---|---|---|
| Metric Q | 5.98 | **9.79** |
| LPC | 0.83 | **0.86** |